Nano Energy 119 (2024) 109050

Contents lists available at ScienceDirect

Nano Energy

journal homepage: www.elsevier.com/locate/nanoen

Dipole-tunable interfacial engineering strategy for high-performance all-inorganic red quantum-dot light-emitting diodes

Fensha Cai [a], Meng Li [a,b,*], Yamei Zhou [a], Yufei Tu [c], Chao Liang [d], Zhenhuang Su [e], Xingyu Gao [e], Zaiping Zeng [a], Bo Hou [f], Zhe Li [b], Mahmoud H. Aldamasy [g], Xiaohong Jiang [a], Shujie Wang [a,**], Zuliang Du [a,**]

[a] Key Lab for Special Functional Materials of Ministry of Education, National & Local Joint Engineering Research Center for High-efficiency Display and Lighting Technology, School of Materials Science and Engineering, and Collaborative Innovation Center of Nano Functional Materials and Applications, Henan University, Kaifeng 475004, China
[b] School of Engineering and Materials Science (SEMS), Queen Mary University of London, London E1 4NS, UK
[c] School of Electronics Information and Intelligent Manufacturing, Sias University, Xinzheng, China
[d] MOE Key Laboratory for Nonequilibrium Synthesis and Modulation of Condensed Matter, School of Physics, Xi'an Jiaotong University, Xi'an 710049, China
[e] Shanghai Synchrotron Radiation Facility (SSRF), Shanghai Advanced Research Institute, Chinese Academy of Sciences, 239 Zhangheng Road, Shanghai 201204, China
[f] School of Physics and Astronomy, Cardiff University, Cardiff, Wales CF24 3AA, UK
[g] Helmholtz-Zentrum Berlin für Materialien und Energie GmbH, Hahn-Meitner-Platz 1, 14109 Berlin, Germany

ARTICLE INFO

Keywords:
All-inorganic quantum dot light-emitting diodes
Interface engineering
NiO_X hole transport layer
Self-assembled monolayer
Molecular dipole

ABSTRACT

All-inorganic quantum dot (QD) light-emitting diodes (AI-QLEDs) with excellent stability received enormous interest in the past few years. Nevertheless, the vast energy offset and the high trap density at the NiO_X/QDs interface limit hole injection leading to fluorescence quenching and hampering the performance. Here, we present self-assembled monolayers (SAMs) with phosphonic acid (PA) anchoring groups modifying NiO_X hole transport layer (HTL) to tune energy level and passivate trap states. This strategy facilitates hole injection owning to the well-aligned energy level by interface dipole, downshifting the vacuum level, reducing the hole injection barrier from 0.94 eV to 0.28 eV. Meanwhile, it mitigates the interfacial recombination by passivating surface hydroxyl group (-OH) and oxygen vacancy (V_O) traps in NiO_X. The electron leakage from QDs toward NiO_X HTL is significantly suppressed. The all-inorganic R-QLEDs exhibit one of the highest maximum luminance, external quantum efficiency and operational lifetime of 88980 cd m^{-2}, 10.3 % and 335045 h (T_{50} @100 cd m^{-2}), respectively. The as-proposed interface engineering provides an effective design principle for high-performance AI-QLEDs for future outdoor and optical projection-type display applications.

1. Introduction

Colloidal quantum dot (QD)-based QLEDs are considered the next-generation light sources due to their high performance, wide-gamut, and facile-solution processability [1–3]. Charge transport layers (CTLs) play essential roles in device performance [4,5]. State-of-the-art QLEDs utilize the most effectively hybrid organic-inorganic CTLs [6,7]. However, organic HTLs suffer from poor photochemical and thermal vulnerability issues, leading to nonreversible degradation [8]. Replacing the organic hole transport materials (HTMs) with inorganic ones is an effective approach for operational stability [9–13]. Among numerous inorganic HTMs, the intrinsic p-type nonstoichiometric NiOx has attracted extensive attention due to its outstanding stability, high optical transmittance, and appropriate work function [14,15].

The AI-QLEDs with NiOx HTL perform much less than conventional QLEDs with hybrid CTLs [16–18]. The main reason is the significant energy barrier between NiO_X and QDs, resulting in insufficient hole injection and increased Auger recombination. In addition, high traps at the NiO_X/QDs interface also serve as non-radiative recombination centers [19]. To overcome such a challenge, ionic doping [20,21], surface

* Corresponding author at: Key Lab for Special Functional Materials of Ministry of Education, National & Local Joint Engineering Research Center for High-efficiency Display and Lighting Technology, School of Materials Science and Engineering, and Collaborative Innovation Center of Nano Functional Materials and Applications, Henan University, Kaifeng 475004, China.
** Corresponding authors.
E-mail addresses: mengli@henu.edu.cn (M. Li), wsj@henu.edu.cn (S. Wang), zld@henu.edu.cn (Z. Du).

https://doi.org/10.1016/j.nanoen.2023.109050
Received 24 July 2023; Received in revised form 27 October 2023; Accepted 28 October 2023
Available online 31 October 2023

treatment [22,23], and insulating insertion layers have been performed to regulate energy-level alignment and inhibit emission quenching [24,25]. Although these strategies can relatively improve the device performance, it still lags behind hybrid CTLs-based QLEDs. Therefore, techniques that simultaneously improve device stability and efficiency must be developed.

Self-assembled monolayers (SAMs) have emerged as the ideal selection to reconcile inorganic surfaces due to their versatility, good surface loading, tunable dipole moment, and high order in photoelectric devices [26–28]. Anchoring groups of SAMs are responsible for binding to the metal or metal oxide surface, which can regulate the work function (WF), tune the shape of the energy barrier at the interface, and passivate trap states [27,29,30]. Terminal groups are responsible for adjusting the surface and interface properties, such as wettability and electronic coupling with the overlayer [28,31,32]. Encouraged by these benefits, the excellent properties of SAMs materials make them promising candidates for NiOx/QDs interface modifications to enhance the AI-QLEDs performance.

In this work, we employed dipole-tunable, PA-based SAMs MeO-2PACz ([2-(3,6-dimethoxy-9 H-carbazol-9-l) ethyl] PA), Me-4PACz ([4-(3,6-dimethyl-9 H-carbazol-9-yl) butyl] PA), and 2PACz ([2-(9 H-carbazol-9-yl) ethyl] PA) as interfacial monolayers to modify NiOx in AI-QLEDs. 2PACz can precisely tune the energy levels for efficient hole injection, as confirmed by the ultraviolet photoemission spectroscopy (UPS) measurements. We studied the carrier dynamics of QDs on NiO_X film with and without SAMs modifications by ultrafast transient absorption (TA) spectroscopy, which revealed a significant reduction of trap states in the interfacial of NiO_X/QDs. Moreover, density functional theory (DFT) calculations showed that oxygen atoms from the phosphoryl group of 2PACz filled the V_O and moved the V_O trap states away from the in-gap region. Accordingly, AI-QLEDs with NiOx/2PACz HTL exhibit a record maximum luminance, peak EQE, and excellent stability of 88980 cd m^{-2}, 10.3 %, and T_{50} @ 100 cd m^{-2} of 335045 h, respectively.

2. Result and discussion

We fabricated AI-QLEDs consisting of multiple layers with ITO/NiO_X/ or NiO_X/SAMs QDs/ZnMgO/Al architecture (Fig. 1**a**). Low-temperature (100 ℃) solution-processed NiO_X nanocrystal films were used as HTL. The SAMs in ethanol were deposited at the surface of NiO_X using spin-coating method, and afterwards, the layers were washed with pure ethanol and annealed to remove all the weakly bonded molecules. CdZnSe/ZnS core/shell QDs with PL emission of 623 nm were used as emitting layer (Fig. S1a). Fig. S1b is the transmission electron microscopy (TEM) image of CdZnSe/ ZnS QDs. The average size of QDs is 15.1 ± 0.5 nm. We used SAMs: MeO-2PACz, Me-4PACz and 2PACz with different molecular dipole moments as interfacial monolayers between NiO_X and QDs to improve the electroluminescence properties. The molecular structures of SAMs are shown in Fig. 1**a**. SAMs molecules are attached to the NiO_X surface by reacting with the hydroxyl groups (-OH). Fig. 1**b** shows the normalized electroluminescence (EL) spectra of AI-QLEDs based on NiO_X and SAM modify NiO_X. The typical EL peak of 2PACz modified-NiO_X-based QLEDs is located at 630 nm with a narrow full width at half-maximum (FWHM) of 24.2 nm, corresponding to the Commission Internationalede l'Eclairage (CIE) color coordinates of (0.68, 0.32), demonstrating high color-saturated red emission. Remarkably, the SAMs-modified devices display FWHM narrower peak than the control device (28.6 nm) and are accompanied by a blue-shift of the peak EL from 642 nm to 630 nm. This could be attributed to the interface engineering alleviated charge imbalance, reducing the generation of Joule heating by non-radiative Auger recombination, thus blue shift EL [33]. The narrower emission for SAMs-modified devices was attributed to the reduction of interfacial defect states, which decreased the luminescence induced by defect states under an applied bias, suggesting more exciton confined in QD and narrowing the FWHM.

Fig. 1**c, d** shows the characteristics of current density-voltage-luminance (*J-V-L*) and EQE-current efficiency-luminance (*EQE-CE-L*) with and without SAMs. The introduction of SAMs gave rise to a significant improvement in EQE and luminance. The turn-on voltage (V_{on}),

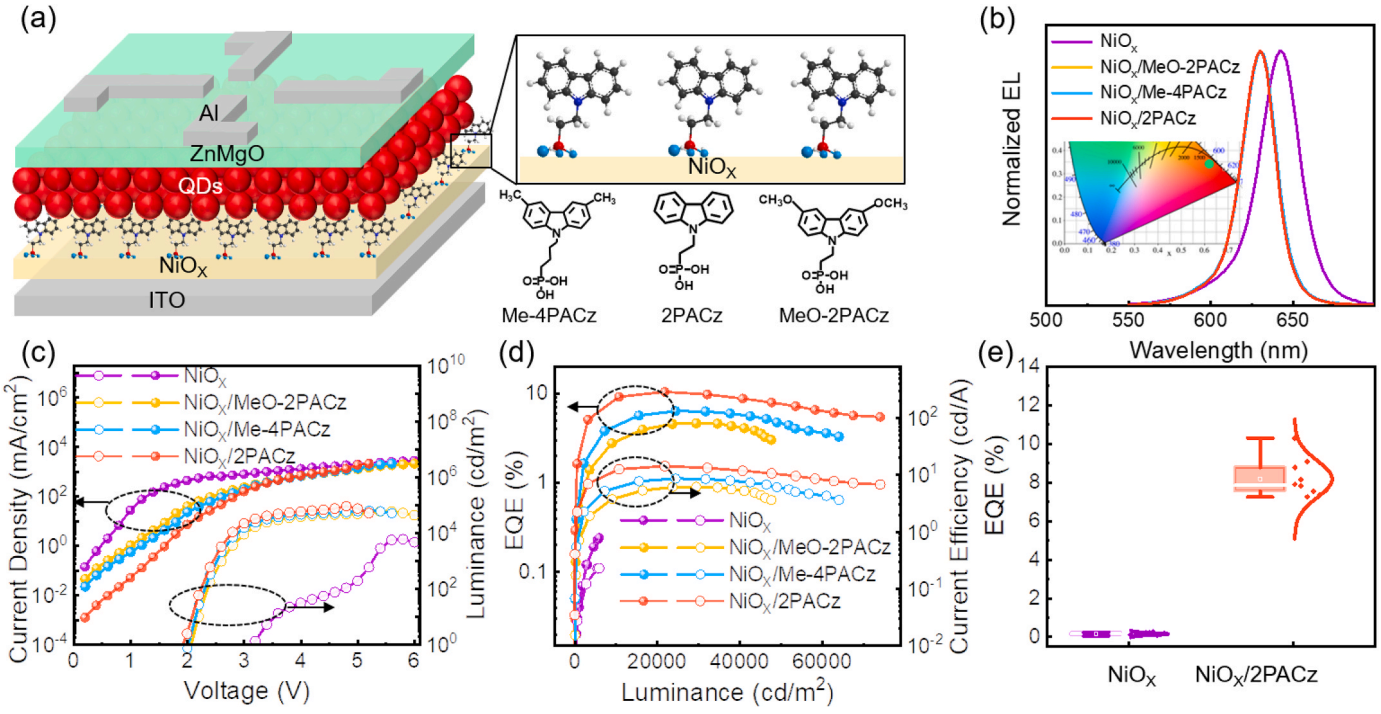

Fig. 1. (a) Schematic illustration of SAMs' device and molecule structures. The zoom-in visualizes SAMs binding to the NiO_X surface. (b) Normalized EL spectra. Inset, CIE coordinate of red AI-QLEDs based on 2PACz modified NiOx HTL. (c) *J-V-L* characteristics, (d) *EQE-CE-L*, and (e) EQE statistics for AI-QLEDs based on NiO_X and NiO_X/SAMs HTLs are shown in boxplots with normal distribution curves.

where the driving voltage attains a 1 cd m^{-2} luminance, decreased from 3.2 V to 1.9 V after modifying NiO_X with 2PACz. The AI-QLEDs based on NiO_X/2PACz showed peak luminance, current efficiency, and EQE of 89880 cd m^{-2}, 14.06 cd A^{-1}, and 10.30 %, respectively. Detailed device parameters are summarized in Table S1. In addition, the EQE distribution features of 10 devices are presented in Fig. 1**e**. The 2PACz-NiO_X-based devices yielded an average EQE of 8.2 % with a relative standard deviation of 0.95 %, outperforming the control devices. We believe that the improvement of device performance results from reducing the energy barrier and facilitating the injection of holes into QDs. Remarkably, the leakage current was considerably reduced by 1–2 orders of magnitude compared to NiO_X-based devices, which is critical to improve performance. We consider that one reason is more holes are injected into QDs recombinating with electrons, alleviating the accumulation of electrons. Another reason is that reducing the electron capture by passivating NiO_X defect states.

To ascertain the reason for performance improvement of AI-QLEDs based on SAMs interfacial modification NiOx HTL, synchrotron-based two-dimensional (2D) grazing incidence X-ray diffraction (GIXRD) was carried out to investigate the QD film's characteristics. Fig. 2**a and b** shows the integrated GIXRD patterns of QDs deposited on NiO_X and NiO_X/2PACz films. The QDs on NiO_X/2PACz exhibited considerably sharper diffraction rings than the control sample, which is attributed to SAM molecules anchored to the NiO_X surface to form strong bonds, reducing interfacial defects and increasing the QD coverage per unit area, thus enhancing the diffraction intensity [34,35]. This was reflected in the out-of-plane line profiles in Fig. 2**c.** The enhanced peak intensities confirmed the better performance of QDs film. Improved performance is known to assist efficient recombination of electrons and holes in QD films, facilitating optimum EL performance of AI-QLEDs [36].

To further verify the interaction between the SAMs and NiOx, we performed X-ray photoelectron spectroscopy (XPS) to evaluate the surface chemistries of NiOx with and without SAMs. The presence of P 2p and N 1 s peaks for the NiO_X/SAM sample at binding energies of 133.2 eV and 400.2 eV from XPS measurements confirmed the binding of SAM on the NiO_X surface (Fig. 2**d, e and** Fig. S2). For clarity, the fine XPS spectra of Ni 2p, O 1 s, and C 1 s have been fitted with multiple Gaussians (Fig. 2**f, S3, and S4**). The O 1 s spectrum of the modified surfaces were fitted with additional C-O-C components (Fig. S4b), which belong to the methoxy groups of MeO-2PACz [37]. Also, the additional C-N, and C-P components were discovered with SAM-modified samples by fitting the C 1 s spectrum (Fig. S3b and S4c). The Ni 2p peak for Ni^{2+} is shifted by 0.36 eV towards higher binding energy after interfacial modification. The homogeneous shift in the binding energy suggested a chemical interaction of SAMs modifying NiO_X. This is ascribed to the PA anchoring group has two hydroxyls and one phosphoryl group, which could anchor on the surface-OH groups of NiO_X with mono-, bi-, and tridentate binding modes (Fig. S5) [23,38]. Due to the presence of molecular dipoles introduced by SAMs, the chemical interaction of SAMs with NiO_X will affect the energy-level alignment at the HTL/QDs interface [38].

We performed UPS to investigate the energy levels of NiO_X with and without SAMs. Fig. 3**a, and b,** Fig. S6a**, and b** display the samples' secondary photoelectron cutoff ($E_{cut\text{-}off}$) and valence band region ($E_{on\text{-}set}$). SAM-treated NiO_X could effectively regulate the energy level. Specifically, the NiO_X with 2PACz interface layer downshifted the valence band maximum (VBM) of pristine NiO_X film from −5.16 eV to −5.82 eV based on the equation: VBM = 21.22 - (E_{cutoff} - E_{onset}). This would significantly lower the hole-injection barrier and establish a better band alignment at the HTL/QDs interface, alleviating the charge imbalance in QDs. The difference in VBM of NiO_X/SAMs is attributed to the different molecular dipole moments of MeO-2PACz, Me-4PACz, and 2PACz. For more details, theoretical DFT calculations were carried out to probe the electronic properties of the three SAMs. SAM's electrostatic potential (ESP) was calculated to determine its electron density distribution (Fig. S7), which strongly depends on the electron-donating ability of the terminal groups [39]. The calculated molecular dipole moment value is ~1.01 D for MeO-2PACz, ~1.6 D for Me-4PACz and ~1.9 D for 2PACz (Fig. S8). The positive dipole shifts the WF of the NiO_X toward higher absolute numbers. Fig. 3**f** illustrates the energy level alignment at the NiOx/QDs interface and 2PACz-modified-NiO_X/QDs interface. 2PACz downshifts the VBM of the NiO_X HTL by 0.66 eV, larger than MeO-2PACz (0.22 eV) and Me-4PACz (0.29 eV) (Fig. S9). The UV–vis absorption spectrum combined with the Tauc plots (Fig. S10) were checked to determine the band gap (E_g) of NiO_X. Data of NiO_X with and without SAM samples extracted from the UV–vis and UPS measurements

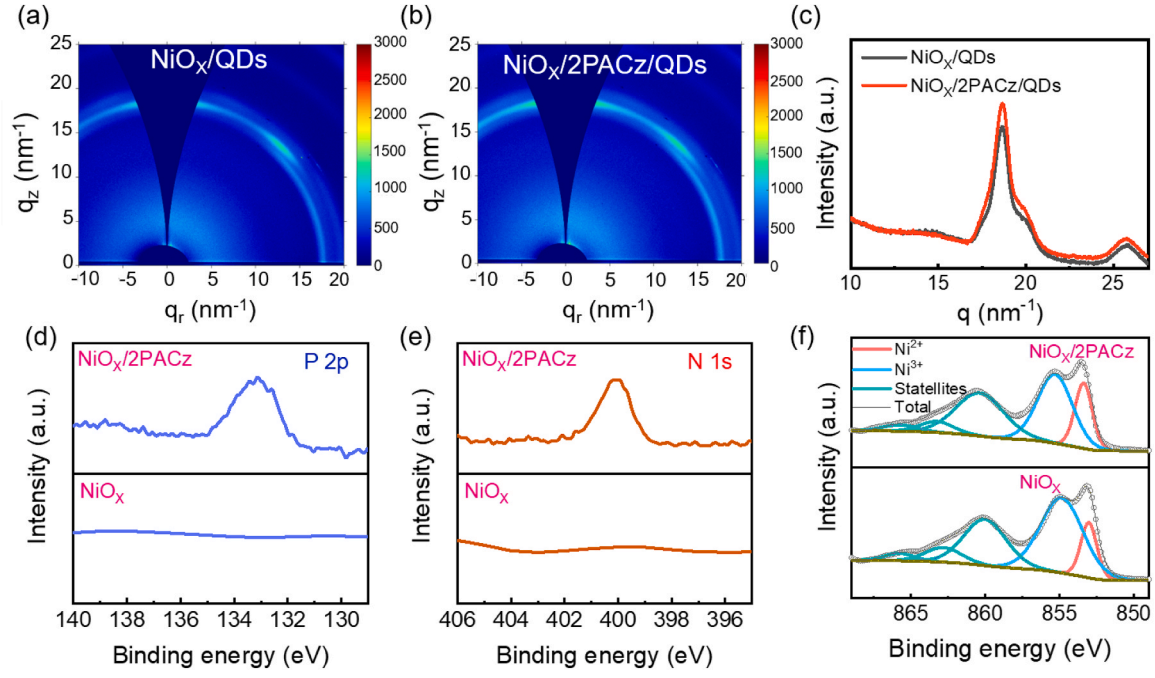

Fig. 2. 2D GIXRD patterns of QDs on (a) NiO_X and (b) NiO_X/2PACz films. (c) Azimuthally integrated 1D plots along the out-of-plane direction. XPS spectra of NiO_X and NiO_X/2PACz surface on ITO for (d) P 2p, (e) N 1 s, and (f) Ni 2p.

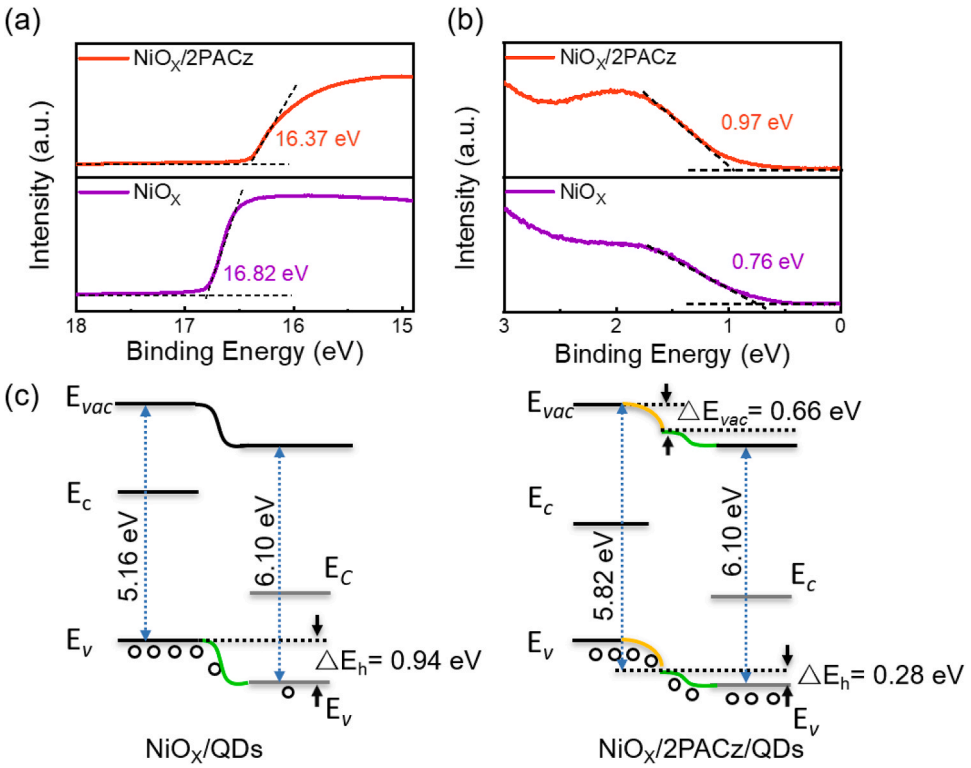

Fig. 3. UPS spectra of NiO_X and NiO_X/2PACz on ITO. (a) the secondary electron cutoff and (b) valence-band edge region. (c) Schematic illustration of energy level alignment at the NiOx/QDs interface (left) and 2PACz-modified-NiO_X/QDs interface (right).

are summarized in Table S2. The schematic illustration of device energy band is shown in Fig. S11**.** In summary, the NiO_X/2PACz HTL has the lowest energy barrier with QDs, reducing the energy barrier from 0.94 eV to 0.28 eV, thus achieves the most improved charge balance, consistent with the above device performance results.

The carrier dynamics of QD films on NiO_X with and without 2PACz treatment were studied by TA spectroscopy. Fig. 4**a, b** shows the TA 2D maps of QD films on NiO_X and NiO_X/2PACz substrates. Both samples show negative values for ground-state bleaching maximum at around 620 nm, which coincides with the exciton absorption position in the steady-state UV–vis absorption spectrum. Fig. 4**c** compares the transition dynamics of QDs on NiO_X and NiO_X/2PACz at 620 nm. For the CdSe-based QDs, the conduction-band electrons overwhelmingly dominate the exciton bleach with negligible contributions from the

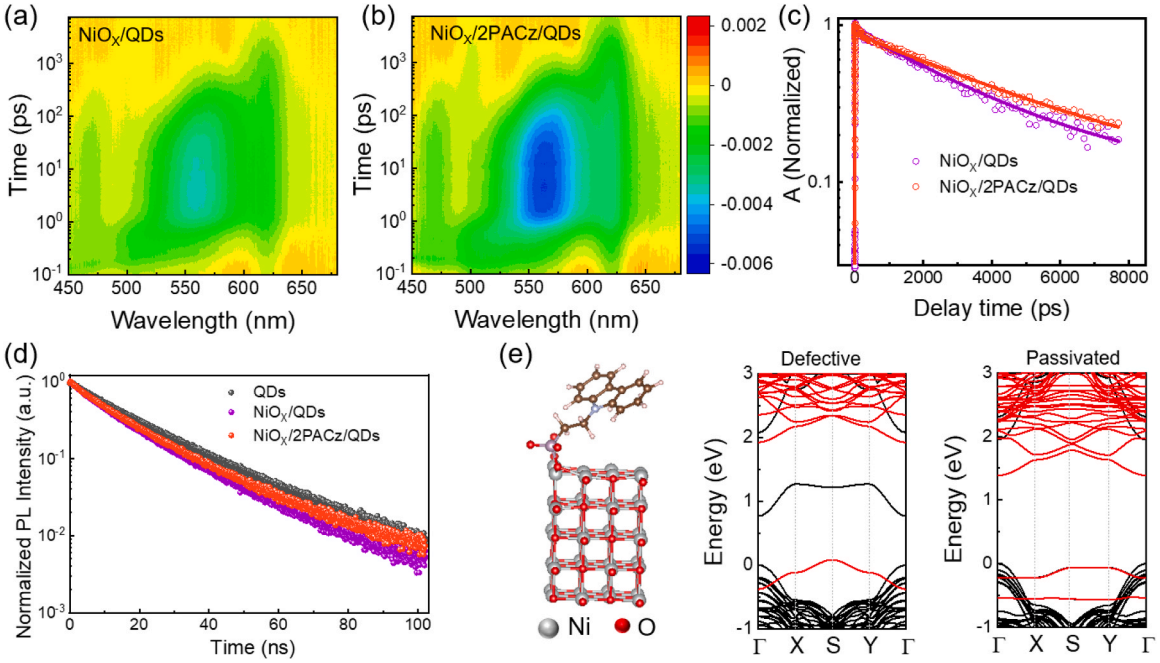

Fig. 4. TA response of (a) NiO_X/QDs and (b) NiO_X/2PACz/QDs films. (c) TA delay at a specific wavelength. (d) TRPL decay for the pristine QDs, NiO_X/QDs, and NiO_X/2PACz/QDs films deposited on quartz substrates. (e) First-principles simulation of passivation effect of 2PACz on NiO_X (V_O) surfaces.

valence-band holes [40,41]. The 2PACz treated sample exhibits a slower delay, indicating a lower electrons capture, which resulting the suppressed exciton quenching in 2PACz treated-NiO_X/QDs interface.

The steady-state PL and time-resolved PL (TRPL) spectroscopy analysis agree with the results of TA kinetics. The QDs on 2PACz-treated NiO_X film show a higher PL intensity than the unmodified sample under the same measurement conditions (Fig. S12). Such a dramatic improvement is attributed to the passivated non-radiative recombination centers at the NiO_X/QDs interface and the enhanced radiative recombination. TRPL spectroscopy curves (Fig. 4**d**) were fitted by a bi-exponential decay model, and the results are shown in Table S3. The average recombination lifetime (τ_{avg}) of NiO_X/QDs films is 12.43 ns, which is lower than QD film (17.57 ns), owing to the exciton quenching by trap states in NiO_X. A prolonged τ_{avg} of 14.93 ns was achieved for 2PACz-treated NiO_X/QDs films. This confirms that 2PACz-treated NiO_X is an effective approach to reduce quenching at the interface by passivating surface-OH. We further carried out DFT method to discover the passivation effect of 2PACz on NiO_X. Our simulation indicates that the V_O, which created more localized in-gap states, is passivated by the phosphoryl group of 2PACz (Fig. 4**e**). The O atom from the phosphoryl group occupied the V_O. It relocated the V_O defect away from the in-gap region, thus reducing trap states density in the interfacial of NiO_X/QDs and enhancing radiative recombination [30,42].

Fig. 5**a and b** illustrates injection and recombination mechanisms for NiO_X-based AI-QLEDs to emphasize the origin of the improved device performance. Overall, SAMs' improved EL performance in SAM-based NiO_X AI-QLEDs is attributed to a bifunctional surface treatment. The interface engineering strategy effectively reduced non-radiative recombination by defect-capturing charge carriers, improved energy-level alignment, and significantly promoted hole injection into QDs. The reduced non-radiative recombination is attributed to the defect passivation of surface-OH and V_O in NiO_X. The improved level alignment results from interfacial dipoles of SAM downshifted the VBM of 0.66 eV, reduced the energy barrier of NiO_X/QD from 0.94 eV to 0.28 eV. To better prove the charge-injection balance, we fabricated single-carrier device of the hole-only devices (HOD) with the structure of ITO/HTLs/QDs/MoO_3/Al and the electron-only devices (EODs) with a structure of ITO/ETL/QDs/ETL/Al (Fig. 5**c**). The current density of HOD based on SAMs-treated NiO_X was 2–3 orders of magnitude higher than that of pristine NiO_X-based HOD, much closer to the electron current. These results reveal that massive hole injection into QDs that could indeed balance the carrier transport, which contributes to achieving highly efficient EL performance.

The device's operational stability was also explored in ambient air (Fig. 5**d**). We observed that the 2PACz treated-NiO_X-based device expands the lifetime. The T_{50} lifetime at an initial luminance of 18430 cd m^{-2} (T_{50}@18430 cd m^{-2}) of AI-QLEDs is determined to be 28.1 h, corresponding to a T_{50}@100 cd m^{-2} of 335045 h or a T_{50}@1000 cd m^{-2} of 5319 h from the empirical equation of $L_0^n T_{50}$ = constant with an acceleration factor (n) of 1.80.[16] The enhanced operational stability is due to decreased non-radiative Auger recombination. The peak EQE and the operational stability of our champion device is one of the highest value among red AI-QLEDs (Fig. S13 **and** Table S4) [16,18,25,43].

3. Conclusion

In summary, we have successfully integrated the SAM as an interface modification interlayer in all-inorganic NiO_X-based red AI-QLEDs. The bifunctional interface engineering strategy favorably regulates the WF of NiO_X by interfacial dipoles and heals the surface defects. The defect states at the interface of NiO_X/QDs can be well passivated by carbazole-based SAMs with PA anchoring groups, which well suppress non-radiative recombination. Benefiting from the improved energy-level alignment, reduced hole injection barrier, and enhanced charge balance, 2PACz modified NiO_X enables the AI-QLEDs with a record-high EQE and luminance of 10.3 % and 89880 cd m^{-2}. More importantly, the AI-QLEDs show a remarkable improvement in operational stability, the superior stability T_{50} @ 100 cd m^{-2} reaches 335045 h. This strategy demonstrates that interface modification provides a simple and efficient way to develop high-performance AI-QLEDs.

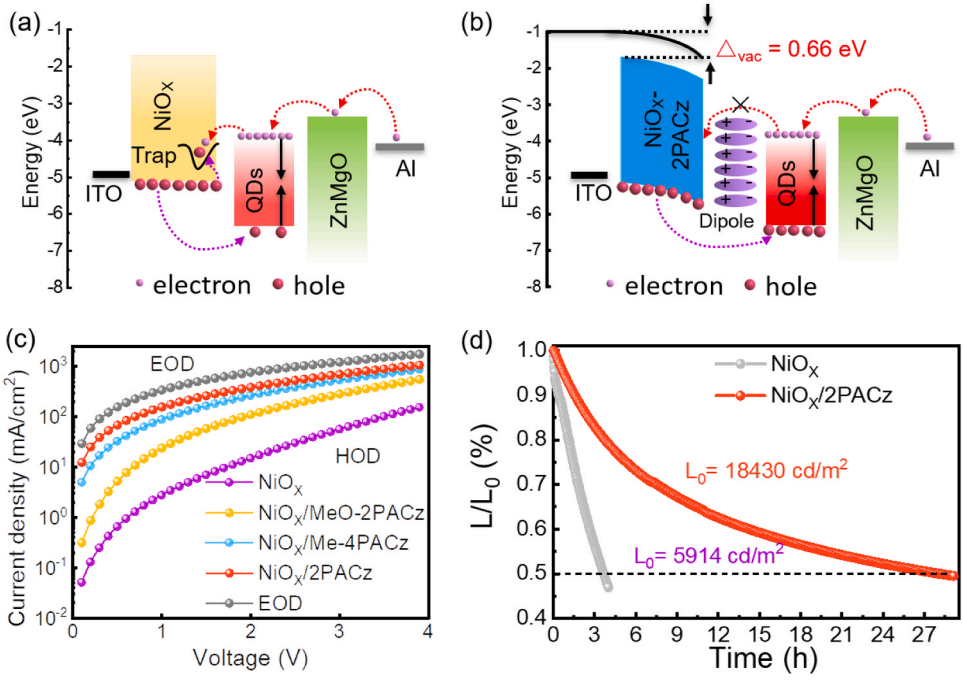

Fig. 5. Schematic illustration of proposed carrier injection and recombination mechanism for (a) NiO_X-based and (b) NiO_X/2PACz-based devices. (c) Current density-voltage characteristics of hole-only devices based on NiO_X and NiO_X/SAMs HTLs. (d) Operational lifetimes of devices based on NiO_X and NiO_X/2PACz HTLs.

CRediT authorship contribution statement

Fensha Cai: Device fabrication, Measurement, Data curation, Writing – original draft. **Meng Li:** Conceptualization, Supervision, Validation, Data curation, Formal analysis, Writing – review & editing. **Yamei Zhou** and **Zaiping Zeng:** Formal analysis, Writing – review & editing. **Chao Liang:** Ultrafast transient absorption (TA) spectroscopy, Funding acquisition. **Zhenhuang Su** and **Xingyu Gao:** Two-dimensional (2D) grazing incidence X-ray diffraction, Writing – review & editing. **Yufei Tu:** Validation, Funding acquisition. **Bo Hou** and **Xiaohong Jiang:** Validation, Supervision, Methodology, Writing – review & editing. **Zhe Li** and **Mahmoud H. Aldamasy:** Validation, Grammar. **Shujie Wang** and **Zuliang Du:** Supervision, Funding acquisition, Formal analysis, Writing – review & editing. All authors discussed the data and commented on the manuscript.

Declaration of Competing Interest

The authors declare that they have no known competing financial interests or personal relationships that could have appeared to influence the work reported in this paper.

Data availability

The authors do not have permission to share data.

Acknowledgements

The authors thank beamline BL14B1 and BL03HB at the Shanghai Synchrotron Radiation Facility (SSRF) for providing the beam time. The authors gratefully acknowledge Professor Chao Liang for providing TA test. This work was supported by the financial support from the National Natural Science Foundation of China (Grant No. 62234006, 62105292, 62374052); National Key Research and Development Program of China (2022YFB3602901); Key Technologies R&D Program of Henan (Grant No. 232102231038); Shanxi Fundamental Science Research Project for Mathematics and Physics (Grant No. 22JSY015).

Appendix A. Supporting information

Supplementary data associated with this article can be found in the online version at doi:10.1016/j.nanoen.2023.109050.

References

[1] H. Shen, Q. Gao, Y. Zhang, Y. Lin, Q. Lin, Z. Li, L. Chen, Z. Zeng, X. Li, Y. Jia, S. Wang, Z. Du, L.S. Li, Z. Zhang, Visible quantum dot light-emitting diodes with simultaneous high brightness and efficiency, Nat. Photonics 13 (2019) 192–197.
[2] B. Li, M. Lu, J. Feng, J. Zhang, P.M. Smowton, J.I. Sohn, I.-K. Park, H. Zhong, B. Hou, Colloidal quantum dot hybrids: an emerging class of materials for ambient lighting, J. Mater. Chem. C 8 (2020) 10676–10695.
[3] A.R.C. Osypiw, S. Lee, S.-M. Jung, S. Leoni, P.M. Smowton, B. Hou, J.M. Kim, G.A. J. Amaratunga, Solution-processed colloidal quantum dots for light emission, Mater. Adv. 3 (2022) 6773–6790.
[4] Z. Zhang, Y. Ye, C. Pu, Y. Deng, X. Dai, X. Chen, D. Chen, X. Zheng, Y. Gao, W. Fang, X. Peng, Y. Jin, High-performance, solution-processed, and insulating-layer-free light-emitting diodes based on colloidal quantum dots, Adv. Mater. 30 (2018) 1801387–1801394.
[5] Y. Ye, X. Zheng, D. Chen, Y. Deng, D. Chen, Y. Hao, X. Dai, Y. Jin, Design of the hole-injection/hole-transport interfaces for stable quantum-dot light-emitting diodes, J. Phys. Chem. Lett. 11 (2020) 4649–4654.
[6] M. Gao, H. Yang, H. Shen, Z. Zeng, F. Fan, B. Tang, J. Min, Y. Zhang, Q. Hua, L. S. Li, B. Ji, Z. Du, Bulk-like ZnSe quantum dots enabling efficient ultranarrow blue light-emitting diodes, Nano Lett. 21 (2021) 7252–7260.
[7] Y.H. Won, O. Cho, T. Kim, D.Y. Chung, T. Kim, H. Chung, H. Jang, J. Lee, D. Kim, E. Jang, Highly efficient and stable InP/ZnSe/ZnS quantum dot light-emitting diodes, Nature 575 (2019) 634–638.
[8] J.H. Chang, P. Park, H. Jung, B.G. Jeong, D. Hahm, G. Nagamine, J. Ko, J. Cho, L. A. Padilha, D.C. Lee, C. Lee, K. Char, W.K. Bae, W. K, Unraveling the origin of operational instability of quantum dot based light-emitting diodes, ACS Nano 12 (2018) 10231–10239.
[9] P. Qin, S. Tanaka, S. Ito, N. Tetreault, K. Manabe, H. Nishino, M.K. Nazeeruddin, M. Gratzel, Inorganic hole conductor-based lead halide perovskite solar cells with 12.4% conversion efficiency, Nat. Commun. 5 (2014) 3834–3839.
[10] F. Cao, Q. Wu, Y. Sui, S. Wang, Y. Dou, W. Hua, L. Kong, L. Wang, J. Zhang, T. Jiang, X. Yang, All-inorganic quantum dot light-emitting diodes with suppressed luminance quenching enabled by chloride passivated tungsten phosphate hole transport layers, Small 17 (2021) 2100030–2100035.
[11] M. Du, S. Zhao, L. Duan, Y. Cao, H. Wang, Y. Sun, L. Wang, X. Zhu, J. Feng, L. Liu, X. Jiang, Q. Dong, Y. Shi, K. Wang, S. Liu, Surface redox engineering of vacuum-deposited NiOx for top-performance perovskite solar cells and modules, Joule 6 (2022) 1931–1943.
[12] E.M. Xuyong Yang, K.D. Cuong Dang, Yuan Gao, Swee Tiam Tan, Xiao Wei Sun, a H.V. Demir, Highly flexible, electrically driven, top-emitting, quantum dot lightemitting stickers, ACS Nano 8 (2014) 8224–8231.
[13] L. Chen, S. Wang, D. Li, Y. Fang, H. Shen, L. Li, Z. Du, Simultaneous improvement of efficiency and lifetime of quantum dot light-emitting diodes with a bilayer hole injection layer consisting of PEDOT:PSS and solution-processed WO3, ACS Appl. Mater. Interfaces 10 (2018) 24232–24241.
[14] J. Lin, X. Dai, X. Liang, D. Chen, X. Zheng, Y. Li, Y. Deng, H. Du, Y. Ye, D. Chen, C. Lin, L. Ma, Q. Bao, H. Zhang, L. Wang, X. Peng, Y. Jin, High-performance quantum-dot light-emitting diodes using NiOx hole-injection layers with a high and stable work function, Adv. Funct. Mater. 30 (2019) 1907265–1907272.
[15] S. Sajid, A.M. Elseman, D. Wei, J. Ji, S. Dou, H. Huang, NiO@carbon spheres: a promising composite electrode for scalable fabrication of planar perovskite solar cells at low cost, Nano Energy 55 (2019) 470–476.
[16] S. Rhee, D. Hahm, H.J. Seok, J.H. Chang, D. Jung, M. Park, E. Hwang, D.C. Lee, Y. S. Park, H.K. Kim, W.K. Bae, Steering interface dipoles for bright and efficient all-inorganic quantum dot based light-emitting diodes, ACS Nano 15 (2021) 20332–20340.
[17] Y. Deng, F. Peng, Y. Lu, X. Zhu, W. Jin, J. Qiu, J. Dong, Y. Hao, D. Di, Y. Gao, T. Sun, M. Zhang, F. Liu, L. Wang, L. Ying, F. Huang, Y. Jin, Solution-processed green and blue quantum-dot light-emitting diodes with eliminated charge leakage, Nat. Photonics 16 (2022) 505–511.
[18] F. Wang, Z. Wang, X. Zhu, Y. Bai, Y. Yang, S. Hu, Y. Liu, B. You, J. Wang, Y. Li, Z. Tan, Highly efficient and super stable full-color quantum dots light-emitting diodes with solution-processed all-inorganic charge transport layers, Small 17 (2021) 2007363–2007373.
[19] L. Tian, R. Tyburski, C. Wen, R. Sun, M. Abdellah, J. Huang, L. D'Amario, G. Boschloo, L. Hammarstrom, H. Tian, Understanding the role of surface states on mesoporous NiO films, J. Am. Chem. Soc. 142 (2020) 18668–18678.
[20] F. Cao, H. Wang, P. Shen, X. Li, Y. Zheng, Y. Shang, J. Zhang, Z. Ning, X. Yang, High-efficiency and stable quantum dot light-emitting diodes enabled by a solution-processed metal-doped nickel oxide hole injection interfacial layer, Adv. Funct. Mater. 27 (2017) 1704278–1704284.
[21] Y. Hou, L.J. Tang, H.W. Qiao, Z.R. Zhou, Y.L. Zhong, L.R. Zheng, M.J. Chen, S. Yang, H.G. Yang, Ni-Co-O hole transport materials: gap state assisted hole extraction with superior electrical conductivity, J. Mater. Chem. A 7 (2019) 20905–20910.
[22] A. Al-Ashouri, E. Kohnen, B. Li, A. Magomedov, H. Hempel, P. Caprioglio, J. A. Marquez, A.B. Morales Vilches, E. Kasparavicius, J.A. Smith, N. Phung, D. Menzel, M. Grischek, L. Kegelmann, D. Skroblin, C. Gollwitzer, T. Malinauskas, M. Jost, G. Matic, B. Rech, R. Schlatmann, M. Topic, L. Korte, A. Abate, B. Stannowski, D. Neher, M. Stolterfoht, T. Unold, V. Getautis, S. Albrecht, Monolithic perovskite/silicon tandem solar cell with >29% efficiency by enhanced hole extraction, Science 370 (2020) 1300–1309.
[23] S. Wang, Y. Li, J. Yang, T. Wang, B. Yang, Q. Cao, X. Pu, L. Etgar, J. Han, J. Zhao, X. Li, A. Hagfeldt, Critical role of removing impurities in nickel oxide on high-efficiency and long-term stability of inverted perovskite solar cells, Angew. Chem. Int. Ed. Engl. 61 (2022) 202116534–202116542.
[24] Y. Jiang, L. Jiang, F.S. Yan Yeung, P. Xu, S. Chen, H.S. Kwok, G. Li, All-inorganic quantum-dot light-emitting diodes with reduced exciton quenching by a MgO decorated inorganic hole transport layer, ACS Appl. Mater. Interfaces 11 (2019) 11119–11124.
[25] X. Yang, Z.-H. Zhang, T. Ding, N. Wang, G. Chen, C. Dang, H.V. Demir, X.W. Sun, High-efficiency all-inorganic full-colour quantum dot light-emitting diodes, Nano Energy 46 (2018) 229–233.
[26] J. Li, H.A. Dewi, H. Wang, J. Zhao, N. Tiwari, N. Yantara, T. Malinauskas, V. Getautis, T.J. Savenije, N. Mathews, S. Mhaisalkar, A. Bruno, Co-evaporated $MAPbI_3$ with graded fermi levels enables highly performing, scalable, and flexible p-i-n perovskite solar cells, Adv. Funct. Mater. 31 (2021) 2103252–2103262.
[27] L. Zuo, Z. Gu, T. Ye, W. Fu, G. Wu, H. Li, H. Chen, Enhanced photovoltaic performance of $CH_3NH_3PbI_3$ perovskite solar cells through interfacial engineering using self-assembling monolayer, J. Am. Chem. Soc. 137 (2015) 2674–2679.
[28] I. Levine, A. Al-Ashouri, A. Musiienko, H. Hempel, A. Magomedov, A. Drevilkauskaite, V. Getautis, D. Menzel, K. Hinrichs, T. Unold, S. Albrecht, T. Dittrich, Charge transfer rates and electron trapping at buried interfaces of perovskite solar cells, Joule 5 (2021) 2915–2933.
[29] Y. Lin, Y. Firdaus, F.H. Isikgor, M.I. Nugraha, E. Yengel, G.T. Harrison, R. Hallani, A. El-Labban, H. Faber, C. Ma, X. Zheng, A. Subbiah, C.T. Howells, O.M. Bakr, I. McCulloch, S.D. Wolf, L. Tsetseris, T.D. Anthopoulos, Self-assembled monolayer enables hole transport layer-free organic solar cells with 18% efficiency and improved operational stability, ACS Energy Lett. 5 (2020) 2935–2944.
[30] L. Li, Y. Wang, X. Wang, R. Lin, X. Luo, Z. Liu, K. Zhou, S. Xiong, Q. Bao, G. Chen, Y. Tian, Y. Deng, K. Xiao, J. Wu, M.I. Saidaminov, H. Lin, C.-Q. Ma, Z. Zhao, Y. Wu, L. Zhang, H. Tan, Flexible all-perovskite tandem solar cells approaching 25%

efficiency with molecule-bridged hole-selective contact, Nat. Energy 7 (2022) 708–717.
[31] S.Y. Kim, S.J. Cho, S.E. Byeon, X. He, H.J. Yoon, Self-assembled monolayers as interface engineering nanomaterials in perovskite solar cells, Adv. Energy Mater. 10 (2020) 2002606–2002626.
[32] E. Aktas, R. Pudi, N. Phung, R. Wenisch, L. Gregori, D. Meggiolaro, M.A. Flatken, F. De Angelis, I. Lauermann, A. Abate, E. Palomares, Role of terminal group position in triphenylamine-based self-assembled hole-selective molecules in perovskite solar cells, ACS Appl. Mater. Interfaces 14 (2022) 17461–17469.
[33] W.K. Bae, Y.S. Park, J. Lim, D. Lee, L.A. Padilha, H. McDaniel, I. Robel, C. Lee, J. M. Pietryga, V.I. Klimov, Controlling the influence of Auger recombination on the performance of quantum-dot light-emitting diodes, Nat. Commun. 4 (2013) 2661–2668.
[34] Y. Cho, J. Lim, M. Li, S. Pak, Z.K. Wang, Y.G. Yang, A. Abate, Z. Li, H.J. Snaith, B. Hou, S. Cha, Balanced charge carrier transport mediated by quantum dot film post-organization for light-emitting diode applications, ACS Appl. Mater. Interfaces 13 (2021) 26170–26179.
[35] M. Li, W.-W. Zuo, Y.-G. Yang, M.H. Aldamasy, Q. Wang, S.H.T. Cruz, S.-L. Feng, M. Saliba, Z.-K. Wang, A. Abate, Tin halide perovskite films made of highly oriented 2D crystals enable more efficient and stable lead-free perovskite solar cells, ACS Energy Lett. 5 (2020) 1923–1929.
[36] P.K. Santra, A.F. Palmstrom, C.J. Tassone, S.F. Bent, Molecular ligands control superlattice structure and crystallite orientation in colloidal quantum dot solids, Chem. Mater. 28 (2016) 7072–7081.
[37] N. Phung, M. Verheijen, A. Todinova, K. Datta, M. Verhage, A. Al-Ashouri, H. Kobler, X. Li, A. Abate, S. Albrecht, M. Creatore, Enhanced self-assembled monolayer surface coverage by ALD NiO in p-i-n perovskite solar cells, ACS Appl. Mater. Interfaces 14 (2022) 2166–2176.
[38] A. Al-Ashouri, A. Magomedov, M. Roß, M. Jošt, M. Talaikis, G. Chistiakova, T. Bertram, J.A. Márquez, E. Köhnen, E. Kasparavičius, S. Levcenco, L. Gil-Escrig, C.J. Hages, R. Schlatmann, B. Rech, T. Malinauskas, T. Unold, C.A. Kaufmann, L. Korte, G. Niaura, V. Getautis, S. Albrecht, Conformal monolayer contacts with lossless interfaces for perovskite single junction and monolithic tandem solar cells, Energy Environ. Sci. 12 (2019) 3356–3369.
[39] J. Qiu, Q. Zhou, D. Jia, Y. Wang, S. Li, X. Zhang, Robust molecular-dipole-induced surface functionalization of inorganic perovskites for efficient solar cells, J. Mater. Chem. A 10 (2022) 1821–1830.
[40] D. Chen, D. Chen, X. Dai, Z. Zhang, J. Lin, Y. Deng, Y. Hao, C. Zhang, H. Zhu, F. Gao, Y. Jin, Shelf-stable quantum-dot light-emitting diodes with high operational performance, Adv. Mater. 32 (2020) 2006178–2006187.
[41] K. Wu, G. Liang, Q. Shang, Y. Ren, D. Kong, T. Lian, Ultrafast interfacial electron and hole transfer from CsPbBr3 perovskite quantum dots, J. Am. Chem. Soc. 137 (2015) 12792–12795.
[42] F. Ali, C. Roldán-Carmona, M. Sohail, M.K. Nazeeruddin, Applications of self-assembled monolayers for perovskite solar cells interface engineering to address efficiency and stability, Adv. Energy Mater. 10 (2020) 2002989–2003012.
[43] Y.-D. Zhang, L. Zhao, Enhanced electroluminescence performance of all-inorganic quantum dot light-emitting diodes: a promising candidate for hole transport layer of Cu-doped NiO nanocrystals, J. Mater. Res. 34 (2019) 2757–2764.